

# Sedimentation dynamics and equilibrium profiles in multicomponent mixtures of colloidal particles

E Spruijt<sup>1</sup> and P M Biesheuvel<sup>2,3</sup>

<sup>1</sup> Institute for Molecules and Materials, Radboud University Nijmegen, Heyendaalseweg 135, 6525 AJ Nijmegen, The Netherlands

<sup>2</sup> Wetsus, Centre of Excellence for Sustainable Water Technology, Agora 1, 8934 CJ Leeuwarden, The Netherlands

<sup>3</sup> Laboratory of Physical Chemistry and Colloid Science, Wageningen University, Dreijenplein 6, 6703 HB Wageningen, The Netherlands

E-mail: [e.spruijt@science.ru.nl](mailto:e.spruijt@science.ru.nl) and [maarten.biesheuvel@wur.nl](mailto:maarten.biesheuvel@wur.nl)


Received 8 July 2013, in final form 14 August 2013

Published 21 January 2014

## Abstract

In this paper we give a general theoretical framework that describes the sedimentation of multicomponent mixtures of particles with sizes ranging from molecules to macroscopic bodies. Both equilibrium sedimentation profiles and the dynamic process of settling, or its converse, creaming, are modeled. Equilibrium profiles are found to be in perfect agreement with experiments. Our model reconciles two apparently contradicting points of view about buoyancy, thereby resolving a long-lived paradox about the correct choice of the buoyant density. On the one hand, the buoyancy force follows necessarily from the suspension density, as it relates to the hydrostatic pressure gradient. On the other hand, sedimentation profiles of colloidal suspensions can be calculated directly using the fluid density as apparent buoyant density in colloidal systems in sedimentation–diffusion equilibrium (SDE) as a result of balancing gravitational and thermodynamic forces. Surprisingly, this balance also holds in multicomponent mixtures. This analysis resolves the ongoing debate of the correct choice of buoyant density (fluid or suspension): both approaches can be used in their own domain. We present calculations of equilibrium sedimentation profiles and dynamic sedimentation that show the consequences of these insights. In bidisperse mixtures of colloids, particles with a lower mass density than the homogeneous suspension will first cream and then settle, whereas particles with a suspension-matched mass density form transient, bimodal particle distributions during sedimentation, which disappear when equilibrium is reached. In all these cases, the centers of the distributions of the particles with the lowest mass density of the two, regardless of their actual mass, will be located in equilibrium above the so-called isopycnic point, a natural consequence of their hard-sphere interactions. We include these interactions using the Boublik–Mansoori–Carnahan–Starling–Leland (BMCSL) equation of state. Finally, we demonstrate that our model is not limited to hard spheres, by extending it to charged spherical particles, and to dumbbells, trimers and short chains of connected beads.

Keywords: sedimentation, centrifugation, multi-component colloidal mixtures, buoyancy, Archimedes, osmotic pressure

 Online supplementary data available from [stacks.iop.org/JPhysCM/26/075101/mmedia](http://stacks.iop.org/JPhysCM/26/075101/mmedia)

(Some figures may appear in colour only in the online journal)

## 1. Introduction

Sedimentation of proteins, colloids and larger particulate matter remains an intriguing and inspiring topic [1–5]. It controls

situations as diverse as the settling of food products [6], such as fruit juices and stocks, sedimentation and syneresis of paints during storage [7], wastewater treatment, the natural accretion of riverbeds [8] and the purification of proteins and

nanoparticles by ultracentrifugation [9]. Despite the wide range of fields in which sedimentation plays a prominent role, some of its aspects, especially in multicomponent mixtures, remain poorly understood. One of the most fundamental puzzles centers around the correct choice of the buoyant density  $\rho_b$  [3], which is the density that must be used to calculate the buoyant force acting on a particle submersed in a fluid that also contains other (colloidal) particles.

When the density distribution of colloidal particles in equilibrium is concerned, it is often asserted that for  $\rho_b$  one must use that of the pure fluid (i.e., that of the liquid, or solvent),  $\rho_F$  [2]. On the other hand, the suspension density,  $\rho_{\text{susp}}$ , is typically used when describing the settling of mesoscopic particles [10–17]. Likewise, the suspension density is used to evaluate the buoyant mass in colloidal suspensions in which one of the particles is much larger than the others, such that the solvent and the small particles together can be thought of as an effective fluid with density  $\rho_{\text{susp}}$ . The suspension density is the volume-averaged density of a mixture, averaging over all particle types, including the fluid,

$$\rho_{\text{susp}} = \sum_i \phi_i \rho_i + (1 - \phi) \rho_F = \rho_F + \sum_i \phi_i (\rho_i - \rho_F) \quad (1.1)$$

where  $\phi_i$  is the volume fraction of particle type  $i$  ( $\phi = \sum_i \phi_i$  is the total particle volume fraction),  $\rho_i$  the particle mass density, and the summation runs over all particle types. If the particle concentrations vary with position, the suspension density becomes a function of position as well. For a one-component system with particles that settle, we have  $\rho_{\text{susp}} > \rho_F$ , and thus, the buoyancy force on a particle, which counteracts gravity, is higher if we assume that  $\rho_b$  is given by  $\rho_{\text{susp}}$  than by  $\rho_F$ .

In this contribution we demonstrate the interrelationship between both approaches mentioned above. As it turns out, the suspension density determines the buoyancy force on a particle, both in and out of equilibrium, but, due to an exactly matching correction of the thermodynamic force that acts on the colloidal particles in equilibrium, the resulting equilibrium sedimentation profile can be calculated using the fluid density as the apparent buoyant density. We emphasize that the approach we follow applies to suspended particles of any size, ranging from ions in density gradient centrifugation to colloidal particles and mesoscopic particles in slurries, and to particles in either monodisperse or polydisperse mixtures. We do not include an arbitrary size criterion to distinguish between large and small particles, as we do not need to combine the latter with the solvent in an effective fluid. Instead, in our approach all particles, small and large, are treated in the same way. Taking this approach, we show how the same theoretical model describes that (1) the suspension density is the buoyant density, while (2) the fluid density can be used to calculate sedimentation profiles in a simplified force balance when sedimentation–diffusion equilibrium (SDE) is reached. This result reconciles theories for equilibrated colloidal suspensions in gravity and centrifugal fields with theories for the dynamics of settling or its converse, creaming, of mesoscopic and granular matter, and resolves the paradox of the correct choice of the buoyant density [2, 18–21].

We demonstrate that the generalized theory we outline predicts the correct equilibrium sedimentation profiles in bidisperse colloidal mixtures by matching predictions to beautiful experimental sedimentation profiles that were recently reported by Piazza and co-workers [1]. To describe the thermodynamic interactions in these mixtures, we use the Boublik–Mansoori–Carnahan–Starling–Leland (BMCSL) equation of state, which has been proven accurate up to considerably high volume fractions (up to  $\sim 0.5$ , [22]). We derive an elegant power series of the BMCSL expression for the excess contribution to the chemical potential of particles in a mixture of many types of particles. As the theory is not limited to equilibrium, our approach also allows calculation of the entire dynamic development of these and other sedimentation profiles. This leads to predictions of sedimentation dynamics that are in qualitative agreement with experiments reported in the literature.

This paper is organized as follows. In section 2 we show how the classical sedimentation–diffusion equilibrium profile follows from a simple force balance in suspensions of monodisperse particles. In section 3 we extend this force balance to a general theoretical framework that describes both equilibrium density profiles and dynamic sedimentation in terms of both potentials and forces for multicomponent mixtures. We apply this framework in section 4 to a model system which consists of a bidisperse mixture of hard spheres. We derive a useful and elegant power series for the equation of state in multicomponent mixtures of hard spheres, and we give analytical expressions for the SDE profiles beyond the tracer limit. In section 5 we turn to sedimentation in centrifugal fields and we discuss a limiting case of the theory presented in the preceding sections. In section 6 we extend our theory to charged colloids and we discuss the assumption of fixed colloidal charge versus that of a regulated colloidal charge. In section 7 we briefly address the particle shape and connectivity as an important factor in the SDE profiles and their dynamic development. We propose a simple modification of the equation of state from section 4 for hard spherical particles that are connected into dumbbells (dimers), trimers and short chains of connected beads, and present calculations of their SDE profiles.

## 2. A simple force balance for hard spheres in equilibrium

We first consider the density profiles of sedimenting, monodisperse hard spheres in equilibrium, based on a simple force balance [1, 23, 24]. We assume that both the particles and the fluid are incompressible and that the particles tend to settle under the influence of gravity. Equilibrium refers to a dynamic state in which the average concentration profiles of the particles do not change, as a result of balancing forces. Each particle is acted on by the body force,  $F^{\text{body}}$ ,

$$F_i^{\text{body}} = -m_i g = -v_i \rho_i g \quad (2.1)$$

where  $m_i$  is the mass of a particle  $i$ ,  $v_i$  the volume ( $v_i = \pi \sigma_i^3 / 6$  for hard spheres),  $\sigma_i$  its diameter,  $\rho_i$  its mass density, and  $g$  the

acceleration due to gravity (here defined as a positive number,  $+9.81 \text{ m s}^{-2}$ ). We choose the upward  $z$ -direction to be opposite to the direction of the gravitational acceleration.

The external body force is balanced by a thermodynamic force  $F_i^{\text{th,tot}}$ , originating from the gradient of the chemical potential  $\mu_i$  of particle type  $i$ , which is a function of both the pressure and the concentration of particles, in the system at constant temperature that we consider here [24]:

$$F_i^{\text{th,tot}} = -\nabla\mu_i = -\left(\frac{\partial\mu_i}{\partial n_i}\right)_{P,T} \nabla n_i - \left(\frac{\partial\mu_i}{\partial P}\right)_{n_i,T} \nabla P \quad (2.2)$$

where  $n_i = \phi_i/v_i$  is the number concentration of species  $i$  and  $\phi_i$  is their volume fraction. For the sedimenting systems considered here, only gradients in  $z$  are relevant. In the second term,  $(\partial\mu_i/\partial P)_{n_i,T}$  is the specific volume of the particles, which is simply their volume  $v_i$  if they are assumed incompressible. The second term can be identified as the buoyancy force, where  $P$  is the hydrostatic pressure  $P^h$ , which is given by [12, 18–20]

$$\frac{\partial P^h}{\partial z} = -\rho_{\text{susp}} g. \quad (2.3)$$

The body force and the buoyancy force are commonly considered in combination, and we define the gravitational force here as a summation of the external body force and the buoyancy force [15, 23]:

$$F_i^{\text{grav}} = -v_i \rho_i g - v_i \frac{\partial P^h}{\partial z} = -v_i (\rho_i - \rho_{\text{susp}}) g = -m_i^b g \quad (2.4)$$

where the buoyant mass  $m_i^b$  is a function of the suspension density.

The first term in equation (2.2) is the concentration-dependent part of the total thermodynamic force [24], and we will refer to that force as the thermodynamic force  $F_i^{\text{th}}$  in this work, omitting the labels for constant temperature from here on:

$$F_i^{\text{th}} = -\left(\frac{\partial\mu_i}{\partial n_i}\right)_P \frac{\partial n_i}{\partial z} = -\left(\frac{\partial\mu_i}{\partial\phi_i}\right)_P \frac{\partial\phi_i}{\partial z}. \quad (2.5)$$

The chemical potential  $\mu_i$  in equation (2.5) is commonly separated into an ideal and an excess contribution ( $\mu_i = \mu_i^{\text{id}} + \mu_i^{\text{exc}}$ ). We note that the thermodynamic force can also be written in terms of an integral over the total pair correlation function  $h(r)$ , as shown by Belloni [25] and Piazza *et al* [1, 21].

In the case of complex mixtures of (possibly soft or charged) particles, explicit expressions for the chemical potential of the particles often do not exist, and in fact, the opposite route is commonly employed: by careful measurements of the sedimentation profiles of colloidal particles in equilibrium, information about the thermodynamic equation of state can be obtained through the  $\mu_i$ 's [26, 27].

It is convenient to write the thermodynamic force in terms of the osmotic compressibility  $(\partial\Pi/\partial\phi_i)_{\mu_F}$ , because this quantity is experimentally accessible by light scattering measurements [28], and because various theoretical expressions exist for the compressibility of suspensions of

hard spheres in a fluid continuum. For the incompressible one-component suspension we consider here, we find (see also supporting information for the general case available at [stacks.iop.org/JPhysCM/26/075101/mmedia](http://stacks.iop.org/JPhysCM/26/075101/mmedia)) [23, 28]

$$\begin{aligned} \frac{1}{v_c} \left(\frac{\partial\mu_c}{\partial\phi}\right)_P &= \frac{1}{v_c} \left(\frac{\partial\mu_c}{\partial\phi}\right)_{\mu_F} - \left(\frac{\partial\Pi}{\partial\phi}\right)_{\mu_F} \\ &= \frac{1-\phi}{\phi} \left(\frac{\partial\Pi}{\partial\phi}\right)_{\mu_F} \end{aligned} \quad (2.6)$$

where the label  $c$  is used to denote the colloidal particles,  $\Pi$  is the osmotic pressure and  $\mu_F$  the chemical potential of the solvent. We note that the derivatives in the rhs of equation (2.6) are understood to be taken at constant chemical potential of the solvent, as is the case when adopting a continuum model for the solvent [29–31]. It is important to distinguish the thermodynamic force as written in equation (2.5), in which the solvent is an explicit component, from the alternative notation of (the contribution to) the thermodynamic force in equation (2.6), in which a continuum model for the solvent is assumed. Transformation between these expressions shows that in the latter case the gradient of the osmotic pressure becomes a natural part of the thermodynamic force acting on the colloids (see supporting information), which gives rise to a factor  $(1-\phi)$  for monodisperse, incompressible suspensions (see equation (2.6)).

Inserting equation (2.6) in equation (2.5) and balancing the thermodynamic force with the gravitational force ( $F_i^{\text{grav}} + F_i^{\text{th}} = 0$ ), leads to:

$$-v_c(\rho_c - \rho_{\text{susp}})g = \frac{v_c(1-\phi)}{\phi} \left(\frac{\partial\Pi}{\partial\phi}\right)_{\mu_F} \frac{\partial\phi}{\partial z}. \quad (2.7)$$

The density difference between the particles and the suspension can be written as  $\rho_c - \rho_{\text{susp}} = (1-\phi)(\rho_c - \rho_F)$  (equation (1.1)), leading to the following well-known differential equation for the density profile of colloids [23, 28, 32]:

$$\frac{1}{\phi} \frac{\partial\phi}{\partial z} = -(\rho_c - \rho_F)g \left(\frac{\partial\Pi}{\partial\phi}\right)_{\mu_F}^{-1}. \quad (2.8)$$

It is important to notice that, even though the buoyancy contribution to the gravitational force (equations (2.3) and (2.4)) depends on the suspension density (as it results from the hydrostatic pressure gradient), the equilibrium sedimentation profile can be calculated by taking the density difference between a particle and the pure solvent as an apparent buoyant density (equation (2.8)). The difference between equations (2.4) and (2.8) originates from a canceling of factors  $(1-\phi)$ . We note that the same differential equation for the sedimentation profile is obtained from the analogous force balance on the solvent (see supporting information).

Equation (2.8) is commonly used as the basis for describing the equilibrium density profiles of suspensions of colloidal particles. In very dilute solutions, the osmotic pressure may be approximated by Van't Hoff's law ( $\Pi = nk_B T$ ) and the

equilibrium density profile is solved analytically to the well-known barometric distribution

$$\lim_{\phi \rightarrow 0} \phi(z) = \phi_0 e^{-z/L_g} \quad (2.9)$$

with the gravitational length

$$L_g = \frac{k_B T}{v_c(\rho_c - \rho_F)g}. \quad (2.10)$$

In more concentrated suspensions of hard spheres the Carnahan–Starling equation of state for hard spheres in a fluid continuum

$$\frac{\Pi}{k_B T} = \frac{\phi + \phi^2 + \phi^3 - \phi^4}{v_c(1 - \phi)^3} \quad (2.11)$$

$$\frac{\mu_c^{\text{exc}}}{k_B T} = \frac{\phi(8 - 9\phi + 3\phi^2)}{(1 - \phi)^3} \quad (2.12)$$

provides a very accurate prediction of the osmotic pressure up to volume fractions as high as 0.5 [22]. The chemical potential in equation (2.12) is related to the osmotic pressure via  $v_c(\partial \Pi / \partial \phi) = \phi(\partial \mu_c / \partial \phi)$ , and is valid within a continuum model for the solvent.

The resulting differential equation for the equilibrium density profile

$$\frac{\partial \phi}{\partial z} = -\frac{1}{L_g} \left( \frac{1}{\phi} + \frac{8 - 2\phi}{(1 - \phi)^4} \right)^{-1} \quad (2.13)$$

has the following solution for  $z(\phi)$  [30, 33]

$$\begin{aligned} \frac{z}{L_g} = & \ln \left( \frac{\phi_0}{\phi} \right) - \frac{1}{(1 - \phi)^2} + \frac{1}{(1 - \phi_0)^2} \\ & - \frac{2}{(1 - \phi)^3} + \frac{2}{(1 - \phi_0)^3} \end{aligned} \quad (2.14)$$

where  $\phi_0$  is the volume fraction at  $z = 0$ .

The approach outlined above, based on a simple force balance for particles in equilibrium, is quite insightful for monodisperse hard spheres under the influence of gravity alone. In the following section we present a more general approach for multicomponent mixtures of (charged) particles in external fields in and out of equilibrium, which simplifies to equation (2.8) for the equilibrium density distribution of a one-component suspension as we have considered here. In view of the applications to bidisperse mixtures of hard spheres, charged colloids and clusters of particles, we will treat the suspending fluid as a continuum in the remainder of this paper, as in the rhs of equation (2.6) [30, 34].

### 3. General theory for sedimentation dynamics and equilibrium density profiles of (colloidal) particle mixtures

#### 3.1. The total potential

The total potential  $\mu_i^{\text{tot}}$  of a particle  $i$  suspended in a continuum fluid can be written as follows

$$\begin{aligned} \mu_i^{\text{tot}} &= \mu_i + \mu_i^{\text{ext}} + \mu_i^{\text{el}} + v_i P^{\text{tot}} \\ &= \mu_i^{\text{id}} + \mu_i^{\text{exc}} + m_i g z + Q_i \psi + v_i P^{\text{tot}} \end{aligned} \quad (3.1)$$

where  $\mu$  is the chemical potential, which can be separated into an ideal contribution  $\mu^{\text{id}}$  and an excess contribution  $\mu^{\text{exc}}$ . The excess contribution is due to volumetric interactions with other particles and can also include activity corrections.  $\mu^{\text{ext}}$  is the contribution due to an external field; in this section we will only consider the field of gravity; hence,  $\mu^{\text{ext}}$  is the contribution due to the body force of equation (2.1).  $\mu^{\text{el}}$  is the contribution due to the electrostatic potential of charged particles in a mean-field approximation. Finally,  $v_i P^{\text{tot}}$  is the insertion energy, required to insert a particle of type  $i$  (volume  $v_i$ ) against the total pressure,  $P^{\text{tot}}$ . Each term will be discussed in turn in this section. This description holds both for dynamically changing situations (i.e., settling particles) and for equilibrium. It can be used for ions, dissolved molecules, colloidal particles, mesoscopic non-colloidal particles, and for any kind of mixture of these particles, regardless of the particle size and shape.

The ideal contribution to the chemical potential of particle of type  $i$  is equal to  $k_B T \ln n_i$ , where  $n_i$  is the number concentration of particles of type  $i$  ( $n_i = \phi_i / v_i$ ). We assume that all particles are incompressible, and hence, the ideal contribution to the chemical potential can be written as

$$\mu_i^{\text{id}} = k_B T \ln \phi_i. \quad (3.2)$$

The excess contribution to the chemical potential describes volumetric interactions between the colloids. This is a key parameter in the description of most sedimentation–diffusion equilibria (SDE) of hard spheres and charged particles and we will discuss our choice for all cases in detail hereafter.

Without any external fields besides gravity, the external potential term is simply

$$\mu_i^{\text{ext}} = m_i g z = v_i \rho_i g z. \quad (3.3)$$

We will discuss how this contribution is modified in a centrifugal field in section 5.

The electrostatic term will be discussed in section 6 in detail. In a mean-field description for particles of fixed charge it is simply  $\mu_i^{\text{el}} = k_B T Z_i y$ , where  $Z_i$  is the charge number of the particle (e.g.,  $\pm 1$  for a monovalent ion),  $Q_i = Z_i e$  and  $y$  the dimensionless electrical potential ( $y = e\psi / k_B T$ ).

Within the continuum model for the fluid, the insertion pressure term is based on the total pressure,  $P^{\text{tot}}$ , which is equal to the local hydrostatic pressure  $P^h$  minus the local osmotic pressure  $\Pi$  [35–42]:

$$P^{\text{tot}} = P^h - \Pi. \quad (3.4)$$

In an equilibrium model, and when the contribution due to gravity can be neglected, such as for the diffuse part of the electrical double layer in Poisson–Boltzmann theory,  $P^h$  will be equal to  $\Pi$ , and as a result, the insertion energy vanishes [41]. If gravity is more prominent, such as in suspensions of sedimenting particles,  $P^h$  is no longer always



equal to  $\Pi$ , and the insertion pressure must be taken into account, as we will describe hereafter<sup>4</sup>. The hydrostatic pressure in a suspension, both in equilibrium and during sedimentation, is given by equation (2.3).

### 3.2. Forces

The expression for the total potential in equation (3.1) can be written in terms of forces, by taking the derivative of equation (3.1) with respect to  $z$ . For the case of uncharged particles, this results in

$$\begin{aligned} F_i^{\text{tot}} &= -\frac{\partial \mu_i^{\text{tot}}}{\partial z} \\ &= -\frac{\partial \mu_i^{\text{id}}}{\partial z} - \frac{\partial \mu_i^{\text{exc}}}{\partial z} - v_i(\rho_i - \rho_{\text{susp}})g + v_i \frac{\partial \Pi}{\partial z} \end{aligned} \quad (3.5)$$

where the term  $v_i(\rho_i - \rho_{\text{susp}})g$  is the gravitational force, which combines the body force  $m_i g$  with the buoyancy force  $v_i(\partial P^h/\partial z)$ , as used already in equation (2.4). The other force elements in equation (3.5), taken together, constitute the thermodynamic force  $F^{\text{th}}$ , which was derived in an alternative way in equation (2.5) (see supporting information). Equation (3.5) applies to both equilibrium sedimentation profiles and settling particles, as long as local thermal equilibrium is assumed.

In SDE, the total force acting on the particles is zero, and the gravitational force is balanced by the thermodynamic force. In that case, we can write the force balance in equation (3.5) more concisely as:

$$F_i^{\text{tot}} = -\frac{k_B T}{\phi_i} \frac{\partial \phi_i}{\partial z} - \frac{\partial \mu_i^{\text{exc}}}{\partial z} - v_i(\rho_i - \rho_F)g = 0 \quad (3.6)$$

using the following expression for the osmotic pressure gradient in SDE (see supporting information) [30]:

$$\frac{\partial \Pi}{\partial z} = -g(\rho_{\text{susp}} - \rho_F). \quad (3.7)$$

We note that equation (3.7) can be used for multicomponent mixtures and for suspensions of charged particles ( $Z_i$  unequal to zero) as well, if we assume local electroneutrality ( $\sum_i n_i Z_i = 0$ ).

In the case of settling particles, the total force is not equal to zero, but it is balanced by a frictional force [15]. We will discuss this friction in more detail in sections 3.3 and 4.2.

Equation (3.5) clearly shows that the buoyancy force is determined by the density of the surrounding suspension. Only in equilibrium are the gravitational and thermodynamic force equal and can the fluid density be used as an apparent buoyant density, see equation (3.6), as discussed in section 2 (equation (2.8)). Interestingly, one can think of various situations in which the thermodynamic force is absent or negligible, and only the gravitational force remains (equation (3.6)). First of all, for particles that are beyond colloidal

dimensions, i.e., mesoscopic or macroscopic particles, the thermodynamic force in equation (3.5) is negligible. Solely the suspension density determines whether these particles move upward ('cream'), or down ('settle') (relative to the solvent velocity). This is a well-known point of view concerning particle sedimentation in engineering fields [11, 13, 16, 17]. Eventually, these particles will stop moving when the gravitational force has vanished, in other words, when their mass density is equal to the local suspension density (the so-called isopycnic point [1]). Secondly, in any suspension, ranging from suspensions of mesoscopic particles, to colloids and even down to mixtures of molecules, the thermodynamic force is absent directly after homogenizing (shaking) the suspension, since all concentration gradients are zero. Hence, only the gravitational force remains, and particles with a density smaller than the (homogeneous) suspension density will initially cream, whereas others will initially settle.

Indeed, a simple but elegant experiment with a suspension containing two types of particles, of which one (polystyrene, PS) has a mass density smaller than the suspension, but larger than the pure solvent, and the other (alumina) has a density larger than the suspension, unambiguously shows that the lighter particles initially cream and, only after the heavier particles have settled and the local suspension density has dropped below that of PS, start to settle themselves [17]. Figure 1 summarizes this process clearly. We emphasize that a choice for the density of the pure fluid in equation (3.5) as the buoyant density would predict that both types of particles would settle directly after shaking, in stark contrast with experimental evidence.

If we continue observing a settling colloidal suspension, we would find that a thermodynamic force gradually develops, from zero directly after mixing, to its final value at equilibrium, where the equilibrium force balance of equation (3.6) holds. We demonstrate this effect in detail in section 4.2, where we consider the application of our approach outlined in this section to a bidisperse mixture of hard spheres.

### 3.3. Dynamic sedimentation

During particle settling, before sedimentation–diffusion equilibrium is reached, the thermodynamic force does not yet balance the gravitational force. Thus, our general equation (3.5) provides the basis for a model to describe particle motion in this situation. We still consider uncharged particles and refer to section 6 for a discussion on charged particles. Before equilibrium is reached, the total force acting on a particle  $i$  in suspension is balanced by a drag (friction) force, which is proportional to the particle's velocity relative to the solvent velocity  $\mathbf{v}_i - \mathbf{v}_F$  in the case that we only consider particle–fluid friction and neglect the effect of acceleration:

$$\begin{aligned} \mathbf{v}_i - \mathbf{v}_F &= \frac{D_i}{k_B T} F_i^{\text{tot}} = -D_i \left( \frac{1}{\phi_i} \frac{\partial \phi_i}{\partial z} + \beta \frac{\partial \mu_i^{\text{exc}}}{\partial z} \right. \\ &\quad \left. + \beta v_i(\rho_i - \rho_{\text{susp}})g - \beta v_i \frac{\partial \Pi}{\partial z} \right) \end{aligned} \quad (3.8)$$

where  $\beta = 1/k_B T$ . The proportionality constant is a diffusion coefficient, which can be approximated by  $D_i = k_B T / 3\pi \eta_F \sigma_i$

<sup>4</sup> The theory presented in our work closely relates to that in [27], which was rigorously based on Maxwell–Stefan theory [82, 83]. The crucial difference is that in [27] the volumetric insertion term  $vP$  (for instance, equation (13) in [27]) is based on  $P^h$ , whereas we argue that it must be based on the total pressure,  $P^{\text{tot}} = P^h - \Pi$ .

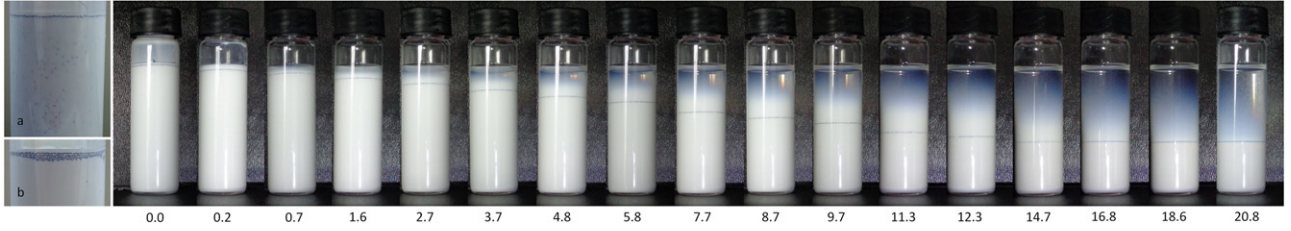


**Figure 1.** Pictures showing the dynamic sedimentation of a bidisperse mixture of alumina (AKP-30, mean diameter  $\sigma = 375$  nm) and a trace amount of PS particles (PB-4, Maxi-Blast Inc., size range  $\sigma = 150\text{--}250$   $\mu\text{m}$ ). Additional details can be found in [17]. The total height of the flask with cap is 63 mm. Within one minute after homogenization, the PS particles that were homogeneously distributed (a), have creamed to the top of the flask (b). Then, they slowly settle as the alumina particles sediment. The numbers below the pictures indicate the time in days after the start of the sedimentation experiment.

with  $\eta_F$  the fluid viscosity, for spherical particles at low Reynolds numbers and low particle concentrations. In the calculations in this paper, we set the particle hindrance functions to unity. These hindrance functions provide a correction to the diffusion coefficient  $D_i$  to account for non-dilute conditions (hydrodynamic effects) [24]. The time-evolution of the particle density profiles can be obtained from the gradient of the volumetric flux  $\phi_i \mathbf{v}_i$  [43]:

$$\frac{\partial \phi_i}{\partial t} = -\frac{\partial}{\partial z}(\phi_i \mathbf{v}_i). \quad (3.9)$$

In a multicomponent mixture of  $N$  types of particles in a common solvent, as many combinations of equations (3.8) and (3.9), combined with the requirement that there is no net flow of the suspension

$$\sum_i \phi_i \mathbf{v}_i + (1 - \phi) \mathbf{v}_F = 0, \quad (3.10)$$

constitute a complete set of equations describing the dynamic sedimentation of these particles. This description is valid for particles of any size, from ions to colloids and mesoscopic particles, and any shape, provided that local thermal equilibrium is satisfied and that the correct equation of state is used to evaluate the osmotic pressure  $\Pi$ , chemical potential  $\mu_i$ , and suspension density  $\rho_{\text{susp}}$  (equation (1.1)) are explicit functions of all  $\phi_i$ . Equation (3.10) ensures a zero net flow of the suspension, which is appropriate in a closed system. In open systems, like sedimentation–filtration set-ups with a continuous flow of fluid [44], and liquid fluidized beds [45], equation (3.10) should be modified to account for net in/outflow of solvent (and/or particles).

#### 4. Application to a bidisperse mixture of hard spheres

In this section we apply the theory outlined in the previous section to a model bidisperse mixture of hard spheres, like the system recently reported by Piazza *et al* [1]. A very small amount of larger particles (poly(methyl methacrylate), PMMA, type 1,  $\sigma_1$  is 440, 600 or 800 nm) is mixed in a suspension of smaller particles (MFA, a trifluoroethylene copolymer, type 2,  $\sigma_2 = 180$  nm). The system is in a so-called

tracer limit, which implies that the presence of the minority species (1) does not influence the sedimentation of the majority species (2) and that interactions between particles of the minority species can be neglected ( $\phi_1 \ll \phi_2$ ).

##### 4.1. Equilibrium density profiles

Piazza *et al* reported that when SDE is reached, an interesting phenomenon is observed. The larger particles (type 1), which have a much larger mass per particle than the smaller particles ( $\pi \sigma_1^3 \rho_1 / 6 > \pi \sigma_2^3 \rho_2 / 6$ ), concentrate in a discrete band at the very top (in the tail) of the distribution of the small majority particles (type 2). The band is located at a height where the local suspension density is distinctly lower than the density of particle 1, in other words, lower than the isopycnic density (see figure 2 in [1]). A similar observation was reported earlier by Morganthaler and Price [46]. These observations suggest that an additional force acts on the large particles, pushing them up [1]. In our view, this must be the thermodynamic force we have discussed in the previous sections, as will be demonstrated here.

In equilibrium the total force on each particle is zero (equation (3.6)). For each particle we thus have a force balance:

$$\frac{\partial \mu_i^{\text{id}}}{\partial z} + \frac{\partial \mu_i^{\text{exc}}}{\partial z} = -v_i(\rho_i - \rho_F)g \quad (4.1a)$$

$$\frac{1}{\phi_i} \frac{\partial \phi_i}{\partial z} + \beta \sum_j \frac{\partial \mu_i^{\text{exc}}}{\partial \phi_j} \frac{\partial \phi_j}{\partial z} = -\frac{1}{L_{g,i}} \quad (4.1b)$$

where  $L_{g,i} = k_B T / v_i(\rho_i - \rho_F)g$  is the gravitational length (see equation (2.10)) and the summation in equation (4.1b) runs over all particle types (including  $i$  itself). Equation (4.1) is an important result, as it shows that not only in a one-component system (one particle plus fluid), but also in a multicomponent mixture, in equilibrium, the density profile can be related directly to the density difference of each particle with the fluid density,  $\rho_F$  (and not  $\rho_{\text{susp}}$ ), whereas all interactions with other particles are included through  $\mu_i^{\text{exc}}$ . Like in the single-component case discussed in section 2, the fact that the SDE density profiles can be related directly to the density difference of each particle with the fluid is the result of a canceling of terms in the thermodynamic and gravitational force.

To describe the excess chemical potential, i.e., the volumetric interactions between the particles in a bidisperse mixture of hard spheres, we will use the Boublik–Mansoori–Carnahan–Starling–Leland (BMCSL) equation of state, which applies to any mixture of hard spheres of unequal sizes.

The BMCSL expressions for osmotic pressure  $\Pi$ , free energy density  $f$ , and chemical potential  $\mu_i$  are given by [47, 48]

$$\frac{\Pi}{k_B T} = \frac{6}{\pi} \left[ \frac{\xi_0}{1-\phi} + \frac{3\xi_1\xi_2}{(1-\phi)^2} + \frac{\xi_2^3(3-\phi)}{(1-\phi)^3} \right] \quad (4.2)$$

$$\frac{f}{k_B T} = \sum_i \frac{\phi_i}{v_i} \ln \frac{\phi_i}{v_i} + \frac{6}{\pi} \left[ -\xi_0 \ln(1-\phi) + \frac{3\xi_1\xi_2}{1-\phi} + \frac{\xi_2^3}{\phi(1-\phi)^2} + \frac{\xi_2^3 \ln(1-\phi)}{\phi^3} \right] \quad (4.3)$$

$$\begin{aligned} \frac{\mu_i}{k_B T} &= \frac{\mu_i^{\text{id}}}{k_B T} + \frac{\mu_i^{\text{exc}}}{k_B T} \\ &= \ln \phi_i - \left( 1 + \frac{2\xi_2^3 \sigma_i^3}{\phi^3} - \frac{3\xi_2^2 \sigma_i^2}{\phi^2} \right) \ln(1-\phi) \\ &\quad + \frac{3\xi_2 \sigma_i + 3\xi_1 \sigma_i^2 + \xi_0 \sigma_i^3}{1-\phi} + \frac{3\xi_2^2 \sigma_i^2}{\phi(1-\phi)^2} \\ &\quad + \frac{3\xi_1 \xi_2 \sigma_i^3}{(1-\phi)^2} - \xi_2^3 \sigma_i^3 \frac{\phi^2 - 5\phi + 2}{\phi^2(1-\phi)^3} \end{aligned} \quad (4.4)$$

where

$$\xi_k = \sum_j \phi_j \sigma_j^{k-3} \quad (4.5)$$

and  $v_i$  is the particle volume ( $v_i = \pi \sigma_i^3/6$  for hard spheres),  $\phi_i$  is the individual particle volume fraction and  $\phi$  is the total particle volume fraction.

The above expression for the excess contribution of species  $i$  to the chemical potential (equation (4.4)) may be expanded into a power series in terms of the total volume fraction  $\phi$  (see supporting information for a derivation):

$$\begin{aligned} \frac{\mu_i^{\text{exc}}}{k_B T} &= \sum_{\lambda=1}^{\infty} \left[ \left( \lambda^2 - 2\lambda - 1 + \frac{2}{\lambda} \right) A^3 + 3 \left( \lambda - \frac{1}{\lambda} \right) A^2 \right. \\ &\quad \left. + 3(\lambda-1)AB + 3A + 3B + C + \frac{1}{\lambda} \right] \phi^\lambda \end{aligned} \quad (4.6)$$

where  $A = \sum_i \alpha_{ij} \zeta_i$ ,  $B = \sum_i \alpha_{ij}^2 \zeta_i$  and  $C = \sum_i \alpha_{ij}^3 \zeta_i$ ,  $\alpha_{ij}$  is the size ratio  $\sigma_i/\sigma_j$ , and  $\zeta_i$  is the relative fraction of each particle type, i.e.,  $\zeta_i = \phi_i/\phi$ . For a one-component suspension, the series in equation (4.6) correctly reduces to the power series expansion of the Carnahan–Starling equation,  $\mu^{\text{exc}} = 8\phi + 15\phi^2 + 24\phi^3 + \dots$  [49], which for low concentrations simplifies to  $\mu^{\text{exc}} = 8\phi$  [50]. For the case that particles of type  $i$  are much smaller than all other particles, we have  $\alpha = 0$ , and equation (4.6) reduces to the power series expansion of the Bikerman equation,  $\mu^{\text{exc}} = \phi + \phi^2/2 + \phi^3/3 + \dots$  [49, 51]. Finally, the limiting form of equation (4.6) in the case that the

particles of type  $i$  are much larger than all other particles (i.e., the ‘colloid-in-electrolyte’ limit) is derived in the supporting information.

In this work especially the tracer limit, in which  $\phi_1 \ll \phi_2$ , is of interest. In this limit the full expression for  $\mu_1^{\text{exc}}$  (derived from equation (4.4)) is given by

$$\begin{aligned} \frac{\mu_1^{\text{exc}}}{k_B T} &= -(1 - 3\alpha^2 + 2\alpha^3) \ln(1 - \phi_2) \\ &\quad + \frac{\alpha\phi_2}{(1 - \phi_2)^3} [5\alpha - 3\alpha\phi_2 + 2 + (3\phi_2^2 - 6\phi_2 + 1)(1 + \alpha - \alpha^2)] \end{aligned} \quad (4.7)$$

where  $\alpha$  now is the size ratio of particle type 1 over 2:  $\alpha = \sigma_1/\sigma_2$ .<sup>5</sup> Note that  $\alpha$  is the same as  $1/q$  in the work of Piazza *et al* [2]. The expansion of equation (4.7) in a power series yields

$$\begin{aligned} \frac{\mu_1^{\text{exc}}}{k_B T} &= \sum_{\lambda=1}^{\infty} [(1 + \lambda\alpha)^3 + 3(\lambda-1)\alpha^2 \\ &\quad + (\lambda-1)(\lambda-2)\alpha^3] \frac{\phi_2^\lambda}{\lambda}, \end{aligned} \quad (4.8)$$

for which the first three terms are

$$\begin{aligned} \frac{\mu_1^{\text{exc}}}{k_B T} &= (1 + \alpha)^3 \phi_2 + ((1 + 2\alpha)^3 + 3\alpha^2) \frac{\phi_2^2}{2} \\ &\quad + ((1 + 3\alpha)^3 + 6\alpha^2 + 2\alpha^3) \frac{\phi_2^3}{3}. \end{aligned} \quad (4.9)$$

A combination of equation (4.8) and the force balance in equation (4.1) leads to an expression for the equilibrium density profile of the minority particles 1. Since we consider the tracer limit,  $\partial\mu_1^{\text{exc}}/\partial\phi_1 = 0$  holds, and we arrive at

$$\begin{aligned} \frac{1}{\phi_1} \frac{\partial\phi_1}{\partial z} + \left( \sum_{\lambda=1}^{\infty} [(1 + \lambda\alpha)^3 + 3(\lambda-1)\alpha^2 \right. \\ \left. + (\lambda-1)(\lambda-2)\alpha^3] \phi_2^{\lambda-1} \right) \frac{\partial\phi_2}{\partial z} = -\frac{1}{L_{g,1}} \end{aligned} \quad (4.10)$$

which can easily be solved for any given gradient of the majority particle. To calculate the equilibrium density profile and the concentration gradient of the majority particles 2, we use the Carnahan–Starling expression for  $\mu_2^{\text{exc}}$  (equation (2.12)) with  $\phi = \phi_2$  to obtain the force balance in equation (3.6) and the density distribution given by equation (2.13).

Figure 2 shows the result of our calculation for the PMMA/MFA system that was recently reported by Piazza *et al* [1]. We take the following parameters from Piazza *et al*:  $\rho_2 = \rho_{\text{MFA}} = 2.14 \text{ g cm}^{-3}$ ,  $\rho_1 = \rho_{\text{PMMA}} = 1.19 \text{ g cm}^{-3}$ ,  $\rho_F = 1.04 \text{ g cm}^{-3}$ ,  $\sigma_2 = 180 \text{ nm}$  and  $\sigma_1 = 440, 600$  or  $800 \text{ nm}$ , resulting in  $L_{g,2} = 124.8 \text{ }\mu\text{m}$  and  $L_{g,1} = 62.7, 24.7$  and  $10.4 \text{ }\mu\text{m}$  for  $\sigma_1 = 440, 600$  and  $800 \text{ nm}$ , respectively ( $T = 298 \text{ K}$ ). Note that we did not use a 10% larger value for  $\sigma_2$  to fit the density profile of MFA particles [1]. Like in figure 2 of

<sup>5</sup> Similar expressions as equations (4.6) and (4.7) are given as equations (6) and (A1) in [49], but there these equations are not correct.

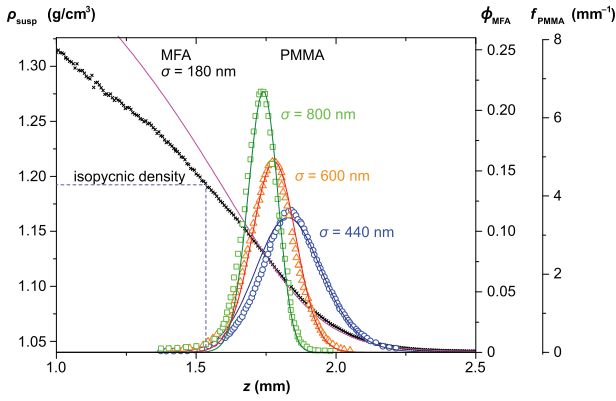


**Figure 2.** Equilibrium sedimentation profiles of various bidisperse suspensions of hard spheres with MFA ( $\sigma_2 = 180$  nm,  $\rho_2 = 2.14$  g cm $^{-3}$ ) always as the majority species and PMMA ( $\sigma_1 = 440, 600$  or  $800$  nm,  $\rho_1 = 1.19$  g cm $^{-3}$ ) as tracers in a solution of urea in water ( $\rho_F = 1.04$  g cm $^{-3}$ ). Symbols are data obtained from turbidity measurements [1].  $f_{\text{PMMA}}$  is the distribution of PMMA colloids (in mm $^{-1}$ ), normalized to 1. Solid lines are theoretical predictions of the density profiles from equations (2.13) and (4.10). The dotted line indicates the isopycnic point for the PMMA particles. Clearly, the maxima of all PMMA density profiles are located above the isopycnic point as a result of excluded volume interactions between the hard spheres.

Piazza *et al* [1] we plot the normalized distribution of each of the three PMMA particles as a function of height  $z$ . It is clear that the theory outlined above accurately describes all tracer particle distributions, with respect to both the location of the bands and the width of the bands. Each fraction of PMMA particle is located in a band with its center of mass far above the isopycnic point. The smaller these minority particles, the higher up the bands are located. In our view, the agreement between our theoretical framework and the experimental data in figure 2 implies that the additional force acting on the large particles and pushing them up to above the isopycnic point is, in fact, the thermodynamic force. This agrees with the expression for the additional force in equation (1) of Piazza *et al* [1], although we would not conclude from this equation that the effective buoyant density is larger than that of the suspension, as is stated at various points in Piazza *et al* [1, 2]. Instead, we argue that the thermodynamic force is due to the gradient in the concentration of the majority (type 2) particles and the associated excluded volume that pushes the minority particles (type 1) up.

In addition to the separate force balances to calculate the equilibrium density profiles, we can combine the two force balances to predict the maximum in the distribution in the tracer particle type 1. At this point  $\partial\phi_1/\partial z = 0$ , and thus, making use of equation (4.1),  $\partial\mu_1^{\text{exc}}/\partial z = (\partial\mu_1^{\text{exc}}/\partial\phi_2)(\partial\phi_2/\partial z)$ . An analytical expression for  $\partial\mu_1^{\text{exc}}/\partial\phi_2$  can easily be derived from equation (4.4), both in the tracer limit and in the general case of mixtures of hard spheres (see supporting information). After inserting the analytical expression for  $\partial\mu_1^{\text{exc}}/\partial\phi_2$  in the tracer limit, expressing  $\partial\phi_2/\partial z$  in terms of  $\mu_2^{\text{exc}}$  using the force balance for type 2 particles (equation (4.1)), and inserting equation (2.12) for  $\mu_2^{\text{exc}}$ , we obtain the following expression

for the particle volume fraction of particles of type 2 at the maximum in the distribution of particles of type 1,  $\phi_2^*$ ,

$$\begin{aligned} \frac{L_{g,2}}{L_{g,1}} &= \alpha^3 \phi_2^{\text{iso}} \\ &= [6\alpha^3 + 2\alpha^3(3-2\alpha)(1-\phi_2^*) + 3\alpha(1-\alpha^2)(1-\phi_2^*)^2 \\ &\quad + (2\alpha^3 - 3\alpha^2 + 1)(1-\phi_2^*)^3]/[\phi_2^{*-1}(1-\phi_2^*)^4 - 2\phi_2^* + 8] \end{aligned} \quad (4.11)$$

where

$$\phi_2^{\text{iso}} = \frac{\rho_1 - \rho_F}{\rho_2 - \rho_F} \quad (4.12)$$

is the ‘isopycnic’ volume fraction of particles of type 2, being the volume fraction of particle type 2 required to have a suspension density equal to the particle mass density of particle type 1, thus where  $\rho_{\text{susp}} = \rho_1$ . Equation (4.11) is in perfect agreement with equation (27) in [21]. Alternatively,  $\partial\mu_1^{\text{exc}}/\partial\phi_2$  can be approximated by the series of powers in equation (4.8), with the corresponding expression for  $\phi_2^*$  given in the supporting information. Taking the limits of  $\alpha \rightarrow \infty$  and  $\phi_2^*$  small, then equation (4.11) simplifies to the expression in [1] (with  $q = 1/\alpha$ )

$$\phi_2^* = \frac{\phi_2^{\text{iso}}}{(1 + \frac{1}{\alpha})^3}. \quad (4.13)$$

We note that equation (4.13) is a simplification obtained under very rigorous assumptions. That equation (4.13) works so well in the data by Piazza *et al* is an amazing surprise. Equation (4.11) is the alternative, complete expression to predict the maximum in the distribution of the tracer particles.

#### 4.2. Dynamic sedimentation

A direct added value of the general theory described in section 3 is that we can also evaluate the dynamics of the settling process in a bidisperse mixture. Combining equations (3.8) and (3.10), and inserting the expression for  $\mu_2^{\text{exc}}$  for the majority particles, type 2 (equation (2.12)), we obtain:

$$\mathbf{v}_2 = -(1-\phi_2)^2 D_2 \left[ \frac{1}{L_{g,2}} + \left( \frac{1}{\phi_2} + \frac{8-2\phi_2}{(1-\phi_2)^4} \right) \frac{\partial\phi_2}{\partial z} \right] \quad (4.14)$$

$$\begin{aligned} \mathbf{v}_1 &= -D_1 \left[ \frac{1}{\phi_1} \frac{\partial\phi_1}{\partial z} - \left( \alpha^3 \left( 1 + \frac{\phi_2(8-2\phi_2)}{(1-\phi_2)^4} \right) - \beta \frac{\partial\mu_1^{\text{exc}}}{\partial\phi_2} \right) \right. \\ &\quad \times \left. \frac{\partial\phi_2}{\partial z} + \frac{\alpha^3(\phi_2^{\text{iso}} - \phi_2)}{L_{g,2}} \right] - \frac{\phi_2 \mathbf{v}_2}{1-\phi_2}. \end{aligned} \quad (4.15)$$

These equations provide a complete set with which the density profile of particles 1 and 2 can be calculated at any point in time. Figure 3 summarizes the resulting dynamics of sedimentation in the system used also in figure 2, but now for several values of the density of the minority particle 1. These plots clearly show the consequences of the definition of the buoyancy force given in equation (2.4). The corresponding movies are included as supporting information.



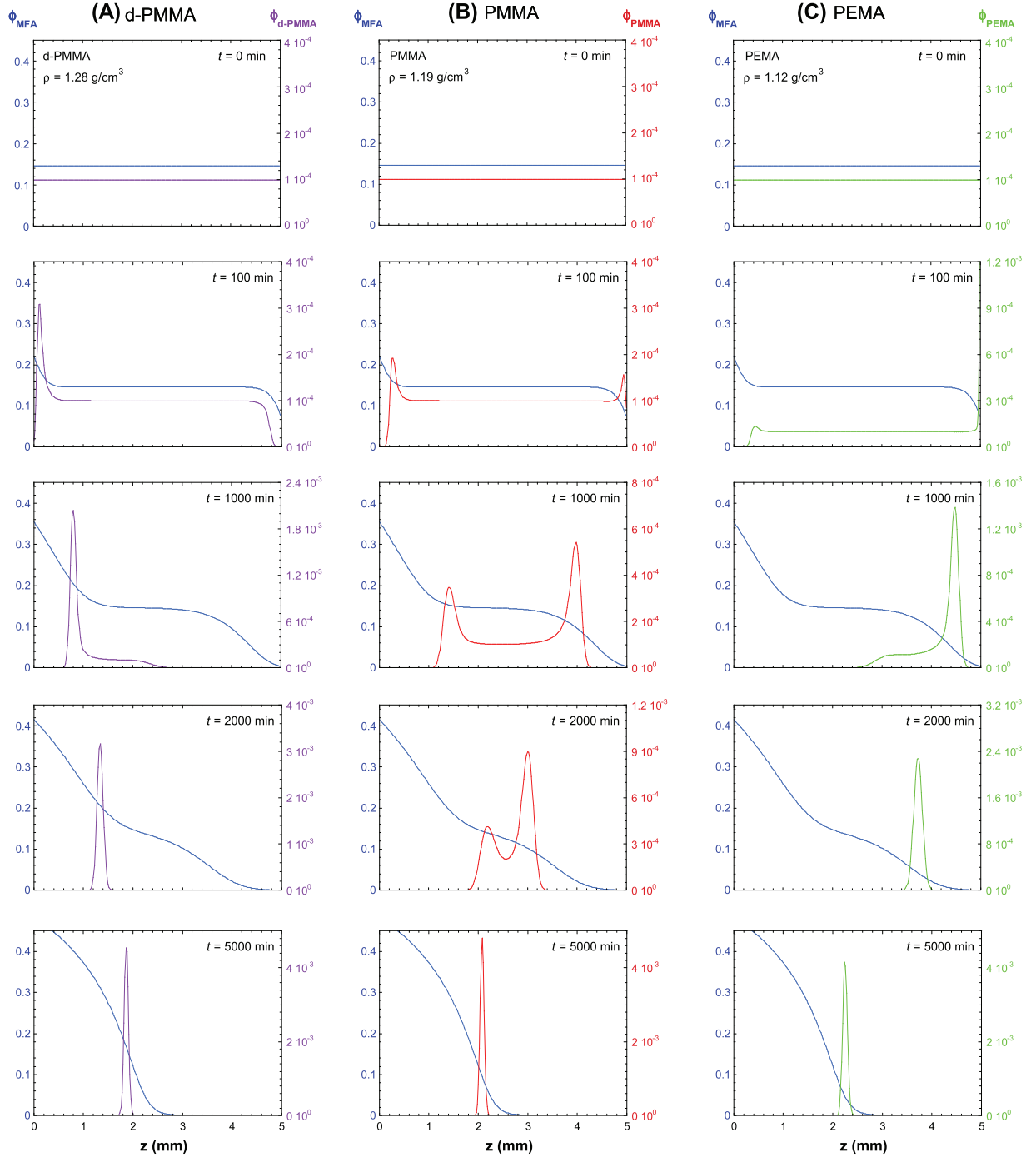


**Figure 3.** Theoretical predictions (equations (4.14) and (4.15)) for the sedimentation dynamics of three types of bidisperse suspensions of hard spheres. In all cases MFA ( $\sigma_2 = 180$  nm,  $\rho_2 = 2.14$  g cm $^{-3}$ ,  $\phi_2$  at  $t = 0$  is 0.145) is the majority component, and the second type of particles ( $\sigma_1 = 1.0$   $\mu$ m, varying density) is present in a trace amount ( $\phi_1$  at  $t = 0$  is  $10^{-4}$ ). The solvent is a solution of urea in water ( $\rho_F = 1.04$  g cm $^{-3}$ ). The suspensions are in a container with a height of 5 mm. Snapshots are shown at  $t = 0, 100, 1000, 2000$  and 5000 min after homogenization. In series A (deuterated PMMA tracers,  $\rho_1 = 1.28$  g cm $^{-3}$ ) the tracer particles have a higher density than the homogeneous suspension ( $\rho_{\text{susp}} = 1.20$  g cm $^{-3}$ ) and they initially settle. In series B (PMMA tracers,  $\rho_1 = 1.19$  g cm $^{-3}$ ) the tracer particles have an almost equal density to the homogeneous suspension and they form a transient bimodal distribution. In series C (PEMA tracers,  $\rho_1 = 1.12$  g cm $^{-3}$ ) the tracer particles have a lower density than the homogeneous suspension and they initially cream.

These dynamic calculations are based on a container of height 5 mm filled with a suspension of MFA ( $\sigma = 180$  nm,  $\rho_2 = 2.14$  g cm $^{-3}$ ) in urea/water ( $\rho_F = 1.04$  g cm $^{-3}$ ) at an initial volume fraction of 0.145, and, hence, the suspension has an average density of 1.185 g cm $^{-3}$ . If we

insert a trace amount of PMMA particles in this container, its density ( $\rho_1 = 1.19$  g cm $^{-3}$ ) would be almost equal to that of the suspension, and, as a result,  $F^{\text{grav}} = 0$  (equation (2.4)). However, as the MFA particles, which have a much higher density than the suspension, start to settle, the local density

at the top of the container drops below that of PMMA, while the local density at the bottom gradually increases due to the settling MFA particles. Consequently, the PMMA particles at the top start to settle and those at the bottom start to cream, giving rise to a transient bimodal particle distribution (see figure 3). Eventually, the peaks meet at the equilibrium height, in agreement with figure 2.

If the PMMA particles are replaced by tracers with a slightly different density, such as poly(ethyl methacrylate) (PEMA,  $\rho_{\text{PEMA}} = 1.12 \text{ g cm}^{-3}$ ), or deuterated poly(methyl methacrylate) (d-PMMA,  $\rho_{\text{d-PMMA}} = 1.28 \text{ g cm}^{-3}$ ), the sedimentation dynamics changes accordingly. In the case we use the heavier d-PMMA particles, they all settle directly from the start, and, while the MFA particles reach their equilibrium density profile, the d-PMMA particles slowly cream to their equilibrium position, which is just below that of the PMMA particles. An illustration of such behavior is given by the experiments recently reported by Parola *et al* [33], where silica particles were found to cream to the top of a diffuse PMMA sediment over a time of 15 days.

In experiments with the lighter PEMA particles, on the other hand, our calculations predict that they first cream to the top of the container, even though their density is larger than the density of the solvent and their size is of the same order of magnitude as the size of the MFA particles. Only after the MFA have started to settle under the influence of gravity, the PEMA particles will settle as well. This prediction is exactly matched by the experimental observations in [17]. The key to this behavior is, as explained above, that the buoyancy force on the PEMA particles is given by the density of the suspension, as opposed to the density of the fluid.

Eventually, all tracer particles reach their equilibrium positions well above the isopycnic point, at a point where the local density is lower than the isopycnic density. The reason for this behavior must be the thermodynamic force that finds its origin in the hard-sphere excluded volume interactions between MFA and tracer particles. The location of the maxima is accurately predicted by equation (4.11). In general, also in multicomponent mixtures of hard spheres beyond the tracer limit (see section 4.3), in equilibrium the centers of mass of the distributions of the particles with the lowest mass density will be located above the isopycnic point. Like for the mixtures with tracer particles, this is a natural consequence of their hard-sphere interactions.

#### 4.3. Beyond the tracer limit

In many suspensions, none of the components is present in trace amounts only, and all volume fractions must be taken into account. As a consequence, the limiting equations (4.7) and (4.10) must be replaced by the full versions in equations (4.1) and (4.4). A convenient way to write these equations in general for a suspension with  $N$  different components was introduced by Biben and Hansen [52] and

Schmidt *et al* [53]:

$$\begin{pmatrix} \mu_{11}(z) & \mu_{12}(z) & \cdots \\ \mu_{21}(z) & \mu_{22}(z) & \\ \vdots & & \ddots \end{pmatrix} \begin{pmatrix} \frac{\partial \phi_1}{\partial z}(z) \\ \frac{\partial \phi_2}{\partial z}(z) \\ \vdots \end{pmatrix} = - \begin{pmatrix} \frac{1}{L_{g,1}} \\ \frac{1}{L_{g,2}} \\ \vdots \end{pmatrix} \quad (4.16)$$

where  $\mu_{ij} = \beta(\partial \mu_i / \partial \phi_j) = (1/\phi_i) + \beta(\partial \mu_i^{\text{exc}} / \partial \phi_i)$  for  $i = j$  and  $\beta(\partial \mu_i^{\text{exc}} / \partial \phi_j)$  for  $i \neq j$ . For the case of mixtures of hard spheres, an analytical expression exists for the partial derivative of the chemical potential ( $\partial \mu_i^{\text{exc}} / \partial \phi_j$ ) (see supporting information). Using standard numerical solution techniques, both the equilibrium sedimentation profiles and the dynamic development of those profiles can be calculated. The full set of equations that was used to do so, is given in the supporting information. We emphasize that the calculations of dynamic sedimentation are an extension of the work in [52, 53], as equation (4.16) only applies in equilibrium.

In figure 4 we show an example of a calculation of the SDE profile for a three-component mixture of hard spheres. The dynamic development of these profiles is visualized in the movies in the supporting information. The initially homogeneous suspension settles under the influence of gravity over a period of weeks (figure 4(a)) into layers of the different particles. With suitable coloring of the particles it would be possible to follow the formation of these bands in detail experimentally.

When the particle densities are chosen such that the light particles have a lower density than the initial suspension, the same phenomenon as in figure 3 can be observed: the lightest particles first cream to the top, revert their motion after some time, and then start settle. However, the dynamic development of the sedimentation–diffusion equilibrium profiles is different from the bidisperse mixture (see supplementary movie 4 available at [stacks.iop.org/JPhysCM/26/075101/mmedia](http://stacks.iop.org/JPhysCM/26/075101/mmedia)). This difference results from the fact that the buoyancy force is determined by the suspension density, as opposed to the fluid density. In a multicomponent mixture, each particle will settle with a different velocity and thus create time-dependent density gradients. More complicated patterns of sedimentation can be achieved in mixtures with even more components, which may also be relevant for manufacturers interested in the shelf life of complex suspensions.

## 5. Application to ultracentrifugation of DNA, proteins and other (bio)colloids

One of the most frequent applications of sedimentation of colloidal mixtures is (analytical) ultracentrifugation of DNA, proteins and subcellular components. Equilibrium sedimentation by centrifugation, which is usually done by density gradient centrifugation, or isopycnic centrifugation, can for instance be used to separate DNA molecules of equal length based on their GC-content [54], to separate RNA from linear DNA, and linear DNA from supercoiled plasmid DNA [55, 56], to purify various proteins, to analyze the binding or complexation of two biomacromolecules [57, 58], and to separate nanorods based on their length and aspect ratio [59]. In ultracentrifugation

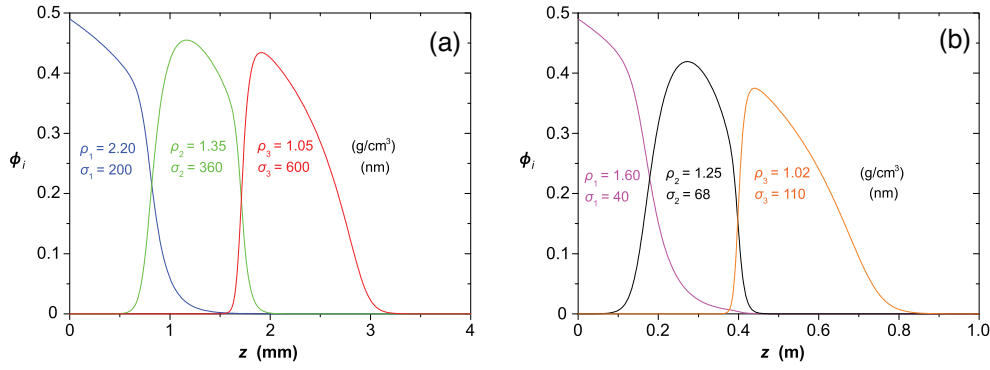


**Figure 4.** Theoretical predictions (equation (4.16)) of the equilibrium sedimentation profiles of two multicomponent mixtures of hard spheres. All species are present in equal and significant amounts. The solvent in both cases is water with  $\rho_F = 1.00 \text{ g cm}^{-3}$ . (a) A three-component mixture with  $\sigma_1 = 200 \text{ nm}$ ,  $\rho_1 = 2.20 \text{ g cm}^{-3}$ ,  $\sigma_2 = 360 \text{ nm}$ ,  $\rho_2 = 1.35 \text{ g cm}^{-3}$ ,  $\sigma_3 = 600 \text{ nm}$  and  $\rho_3 = 1.05 \text{ g cm}^{-3}$ . The total sedimentation profile extends to a height  $z$  of  $\sim 3 \text{ mm}$ . (b) A three-component mixture with  $\sigma_1 = 40 \text{ nm}$ ,  $\rho_1 = 1.60 \text{ g cm}^{-3}$ ,  $\sigma_2 = 68 \text{ nm}$ ,  $\rho_2 = 1.25 \text{ g cm}^{-3}$ ,  $\sigma_3 = 110 \text{ nm}$  and  $\rho_3 = 1.02 \text{ g cm}^{-3}$ . The total sedimentation profile extends to a height  $z$  of  $\sim 80 \text{ cm}$ .

the process of sedimentation takes place in a centrifugal field with an effective strength that is much larger than that of the gravitational field considered in the previous sections. The theory presented in the previous sections can, however, still be applied to calculate the equilibrium sedimentation profiles and dynamics of sedimentation, if the centrifugal field is taken into account in  $\mu_i^{\text{ext}}$  and  $P^h$  in equation (3.1). Then, the centrifugal force, which combines the body force  $m_i \omega^2 r$  and the buoyancy force  $v_i (\partial P^h / \partial r)$ , analogous to the gravitational force, is

$$F_i^{\text{centr}} = -v_i \rho_i \omega^2 r - v_i \frac{\partial P^h}{\partial r} = -v_i (\rho_i - \rho_{\text{susp}}) \omega^2 r \quad (5.1)$$

$$\mu_i^{\text{centr}} = \frac{m_i \omega^2 r^2}{2} + v_i P^h = \frac{v_i \rho_i \omega^2 r^2}{2} + \int \rho_{\text{susp}}(r) \omega r dr \quad (5.2)$$

where  $\omega$  is the angular velocity of the centrifuge (in  $\text{rad s}^{-1}$ ),  $r$  is the distance to the center of the centrifugal axis, and the equivalent field strength is expressed by  $\omega^2 r$  (relative centrifugal force, rcf), or sometimes by  $30\omega/\pi$  (revolutions per minute, rpm). Similar to the body force (and potential), the centrifugal field must be taken into account in the hydrostatic pressure gradient as well (see equation (2.3)), and, thus, the total force for the case of uncharged particles in a centrifugal field becomes (see supporting information for more details):

$$\begin{aligned} F_i^{\text{tot}} &= -\frac{\partial \mu_i^{\text{tot}}}{\partial z} \\ &= -\frac{\partial \mu_i^{\text{id}}}{\partial z} - \frac{\partial \mu_i^{\text{exc}}}{\partial z} - v_i (\rho_i - \rho_{\text{susp}}) \omega^2 r + v_i \frac{\partial \Pi}{\partial z}. \end{aligned} \quad (5.3)$$

Typically, the forces generated by the centrifugal fields that are used for instance to separate DNA molecules or proteins, are the equivalent of  $10^5$ – $10^6 \text{ g}$ . Consequently, for most particles other than small molecules (for which  $v_i$  is small enough) the centrifugal contribution to the total force

dominates the thermodynamic forces ( $-\partial \mu_i / \partial z$ ) and any possible other corrections due to particle charges (DNA) or other soft particle interactions. Hence, for DNA, proteins, membranes, colloids, and other particles the total force can safely be simplified to

$$F_i^{\text{tot}} \approx -v_i (\rho_i - \rho_{\text{susp}}) \omega^2 r. \quad (5.4)$$

As a logical result, these particles will come to a halt ( $F_i^{\text{tot}} = 0$ ) when their density is equal to the density of the surrounding suspension, hence the name isopycnic centrifugation.

In density gradient centrifugation the varying density in the direction of the centrifugal force is typically generated by small molecules, such as cesium chloride ( $\sigma_{\text{Cs}} \approx 0.34 \text{ nm}$ ) or sucrose ( $\sigma_{\text{sucr}} \approx 0.92 \text{ nm}$ ), or small particles such as Percoll (silica of  $\sigma \approx 10 \text{ nm}$  coated with poly(vinyl pyrrolidone)). A crude estimate of the width of the sedimentation profiles of these small molecules can be obtained from the so-called centrifugal length  $L_\omega$ , which is the centrifugal equivalent of the gravitational length in equation (2.10)

$$L_\omega = \sqrt{\frac{k_B T}{v_c (\rho_c - \rho_F) \omega^2}}. \quad (5.5)$$

In a typical density gradient centrifugation experiment, based on cesium chloride with a centrifugal acceleration of  $\omega^2 r = 2 \times 10^5 \text{ g}$  ( $r = 25 \text{ cm}$ ), the density gradient of the heavy cesium ions will be significant for a typical centrifuge tube, based on the estimated  $L_{\omega, \text{Cs}} = 5.1 \text{ cm}$  ( $\sigma_{\text{Cs}} = 0.34 \text{ nm}$ ,  $M_{\text{Cs}} = 132.9 \text{ g mol}^{-1}$ ). In agreement with the theory in the previous sections, a thermodynamic force will oppose the sedimentation of the cesium ions, leading to a characteristic SDE density profile. In this case, hard-sphere interactions alone cannot fully describe the sedimentation profile. Most importantly, the cesium ion concentrations will be strongly correlated with the chloride ion concentrations as a result of electroneutrality, which will mutually affect the sedimentation profiles of cesium and chloride ions. In a sucrose gradient, the estimated

centrifugal length at similar centrifuge settings is  $L_{\omega, \text{sucr}} = 5.7 \text{ cm}$  ( $\sigma_{\text{sucr}} = 0.92 \text{ nm}$ ,  $M_{\text{sucr}} = 342 \text{ g mol}^{-1}$ ).

Nonetheless, exact calculation of the thermodynamic force is often not necessary in density gradient centrifugation to determine the equilibrium profiles of the biomolecules or colloids of interest, since they will end up at the point where their density is matched with the density of the surrounding (cesium chloride or sucrose) solution (see equation (5.4)) and the local density can be measured by refractive index measurements of the solution or by weighing successive aliquots of equal volume from the gradient.

Analytical ultracentrifugation can also be used to obtain information about the size, shape and effective density of a particle without density gradients (in pure water for instance). Application of equation (3.8) to a particle in a centrifugal field yields a characteristic sedimentation velocity as a function of buoyant mass and size of the particle

$$\mathbf{v}_i - \mathbf{v}_F \approx \beta D_i v_i (\rho_i - \rho_{\text{susp}}) \omega^2 r. \quad (5.6)$$

In experiments without density gradients the sedimentation velocity is approximately constant, after a short startup time. It is common to report sedimentation coefficients instead of sedimentation velocities. Sedimentation coefficients  $s$  are defined as the terminal sedimentation velocity (approximated by equation (5.6)) normalized by the applied acceleration ( $\omega^2 r$ ).

$$s_i = \frac{\mathbf{v}_i}{\omega^2 r} \approx \beta D_i v_i (\rho_i - \rho_{\text{susp}}) + \frac{\mathbf{v}_F}{\omega^2 r} \quad (5.7)$$

which leads to the well-known Stokes sedimentation coefficient in the dilute limit ( $\phi \rightarrow 0$ ) for the Stokes–Einstein approximation of the diffusion coefficient:  $s_i = \sigma_i^2 (\rho_i - \rho_F) / 18 \eta_F$ . Sedimentation coefficients have units of time (Svedberg or second,  $1 \text{ S} = 10^{-13} \text{ s}$ ). Theoretical considerations that link the sedimentation coefficients to particle density, size and shape date back to Svedberg [28, 60], who mostly considered the ratio  $s_i / D_i$  in dilute limits. We note that in the more general case of sedimenting particles, the density of the suspension and the diffusivity of the particles in suspension are the relevant parameters that govern the sedimentation behavior of particles in a centrifugal field, in agreement with the general force balance in equations (3.5) and (3.8). In simple, single-component suspensions of hard spheres, however, the sedimentation coefficient of the colloidal particles may also be calculated using the fluid density (see supporting information) [28].

Finally, the dynamics of sedimentation in an ultracentrifuge can also be used to separate particles with identical densities but different sizes or shapes [61, 62]. Particles with different sizes and shapes will differ in their characteristic sedimentation velocity  $\mathbf{v}_i$  and diffusivity  $D_i$ . Initially homogenized mixtures of these particles may thus separate into temporary bands during sedimentation [61], which can be isolated for further studies.

## 6. Application to charged colloids

So far we have limited our theory to particles that only interact as hard spheres. However, when the particles are

charged, and the ionic strength of the solvent is low, the sedimentation–diffusion equilibrium (SDE) profile becomes strongly inflated because gravity (centrifugation) must not only compete with the entropy of the colloids, but with those of the ions as well [30, 63–65]. In this section we analyze how the presence of charges on the colloids modifies the theory outlined in the previous sections. We use a set of experimental data on charged silica particles ( $\sigma \approx 40 \text{ nm}$ ) in ethanol in a centrifugal field from [26, 66]. We will use these data to show the differences in the predicted behavior between particles with a fixed charge and particles with a charge that depends on the local concentration of ions and colloids.

The experimental sedimentation profiles of charged silica particles, which are based on the data in figure 11 of [66] and corrected for the actual size of the silica particles, are shown in figure 5(a). These sedimentation profiles are strongly inflated due to the electrostatic interactions between the particles, as can be seen from the corresponding theoretical sedimentation profile of uncharged hard spheres with the same centrifugal length, depicted at the very left in figure 5(a). The sedimentation–diffusion equilibrium profiles and the osmotic pressure of the one-component suspension of charged silica particles (we neglect the effect of gravity on the ions) are interrelated via [27, 63, 67–72]

$$\frac{\partial \Pi}{\partial r} = \frac{n(r) k_B T r}{L_\omega^2} = \phi (\rho_c - \rho_F) \omega^2 r \quad (6.1)$$

where  $n(r)$  is the colloid number density,  $\omega$  is the centrifugal speed (in  $\text{rad s}^{-1}$ ),  $r$  is the radial coordinate,  $L_\omega$  is the centrifugal length (see equation (5.5)) and the label  $c$  is used to denote the colloidal particles.

In equilibrium, the total potential of the particles (see equation (3.1)) is constant with height. For charged particles the electrostatic contribution to the total potential must be taken into account explicitly. If the charge of the particles is a function of the local concentration of ions (including protons as the most common charge-determining ions), it thus depends on the local electrostatic potential  $\psi$  (or  $y$ ), and an additional equation is needed to take this charge regulation into account, as discussed in detail in [63].

In the derivation of the equation of state for charged colloids in suspension, we use a mean-field approach, as was done in the thermodynamic derivations in the previous sections as well. We further assume that the colloids are very dilute ( $\mu_i^{\text{exc}} = 0$ ), which is supported by experiments (see figure 5(a)), and we assume that a condition of local electroneutrality holds at each height in the column, which is a reasonable assumption throughout the bulk of the sedimenting sample, except very close to the top and bottom walls [65, 73]. Hence, at each height

$$\frac{Z\phi}{v_c} - 2n_\infty \sinh y = 0 \quad (6.2)$$

holds, where  $n_\infty$  is the ionic strength of the suspension, evaluated in the absence of colloids (i.e., in the supernatant), assuming that all ions are monovalent, fully dissociated, and Boltzmann distributed in the potential field without volumetric



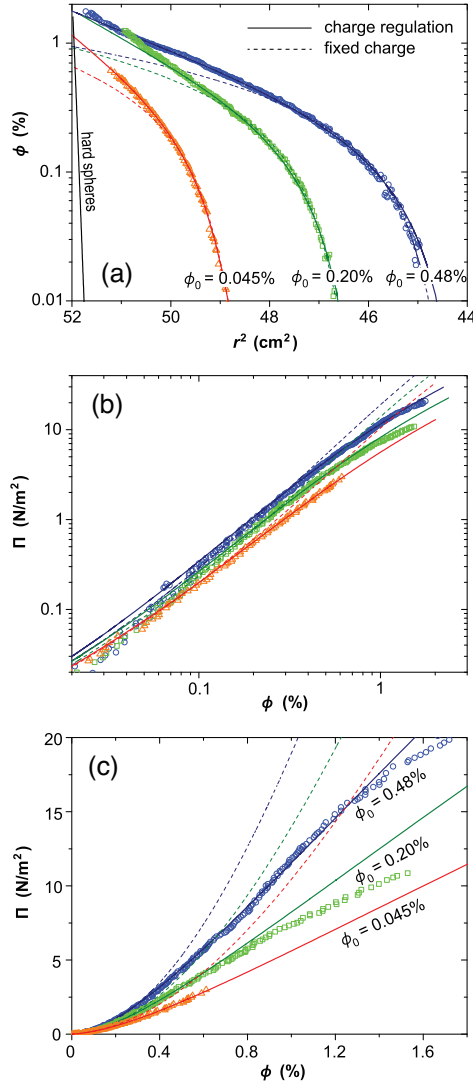


**Figure 5.** (a) Centrifugal sedimentation–diffusion equilibrium density profiles for  $\sigma = 43.8$  nm silica particles in ethanol ( $L_\omega = 2.94$  mm) at different values of the ionic strength, as a result of different average volume fractions of colloids:  $\phi_0 = 0.045\%$  corresponds to  $\kappa^{-1} = 56$  nm,  $\phi_0 = 0.20\%$  to  $\kappa^{-1} = 47$  nm and  $\phi_0 = 0.48\%$  to  $\kappa^{-1} = 39$  nm [26, 63]. The black line close to the left vertical axis is a theoretical sedimentation profile of uncharged hard spheres with the same centrifugal length  $L_\omega$ . (b) Osmotic pressure (equation (6.1)) data as a function of volume fraction  $\phi$  for the data in (a) on a double-logarithmic scale. (c) The same on a linear scale. All dashed lines are fits to a model that assumes a fixed colloid charge (with  $Z_c = 33, 46$  and  $65$  for  $\phi_0 = 0.045\%, 0.20\%$  and  $0.48\%$  respectively); solid lines are fits to a model that includes charge regulation (with  $Z_\infty = 35, 54$  and  $79$ ).

interactions and no centrifugal force acting on them. Using equation (6.2), the local electrostatic potential  $\psi$  (or  $y$ ) in equation (3.1) can be written as a function of the colloid volume fraction  $\phi$ .

The osmotic pressure of a colloidal mixture of particles of a fixed colloid charge,  $Z_c$ , is given by [74–77]

$$\frac{\Pi_c}{k_B T} = \frac{\phi}{v_c} + 2n_\infty \left[ \sqrt{1 + \left( \frac{Z_c \phi}{2n_\infty v_c} \right)^2} - 1 \right]. \quad (6.3)$$

If instead, the charge of the colloids is regulated by the local ion concentration, according to a simple Langmuir isotherm in the limit of a low ionization degree, equation (6.3) must be replaced by [63]

$$\frac{\Pi_c}{k_B T} = \frac{\phi}{v_c} + 2n_\infty \left[ \frac{X + X^{-1}}{2} - 1 \right] \quad (6.4)$$

with

$$X = \sqrt{1 + \frac{Z_\infty \phi}{n_\infty v_c}} \quad (6.5)$$

where  $Z_\infty$  is the charge of the colloids at infinite colloid dilution ( $\phi \rightarrow 0$ ). As the concentration of colloids increases, the actual charge  $Z_r(\phi)$  becomes less than  $Z_\infty$ , according to

$$Z_r(\phi) = Z_\infty \sqrt{\frac{n_\infty v_c}{n_\infty v_c + Z_\infty \phi}}. \quad (6.6)$$

As an example, for one data set in figure 5 we estimate that the charge of  $\sigma = 44$  nm colloids in suspension with an ionic strength  $n_\infty = 10^{-5} \text{ nm}^{-3}$  ( $\kappa^{-1} = 39$  nm) decreases from  $Z_r = 79$  at infinite dilution to  $Z_r = 25$  when the particles are compressed to  $\phi = 5\%$ . Equation (6.6) also shows that when the ionic strength  $n_\infty$  increases, the charge reduction upon increasing  $\phi$  is suppressed. We note that the model for charge regulation has the same number of free parameters as the model for a fixed colloid charge.

In figure 5 we compare the model assuming a fixed particle charge, and the model assuming charge regulation, with the data. We use values for the ionic strength (via Debye length,  $\kappa^{-1}$ ) as shown in table 1 of [63], and a value of  $L_\omega = 2.94$  mm, based on a measured value for the particle diameter  $\sigma = 43.8$  nm, for all data sets. Figure 5(b) shows osmotic pressure data and theoretical predictions on a double-logarithmic scale. Both the model with a fixed charge and the model with a regulated charge seem to describe the data quite well. However, when we look at the same data on a linear scale in figure 5(c) we see a significant deviation at high  $\phi$  ( $\phi > 0.35\%$ ) for the fixed charge model, as also observed in [66]. On the other hand, the model including charge regulation remains very accurate up to much higher concentrations: up to  $\phi \approx 1.4\%$  for the  $\phi_0 = 0.48\%$  dataset. At even higher  $\phi$  equation (6.4) overestimates the osmotic pressure, suggesting that either the charge of the colloids decreases more rapidly than predicted by equation (6.4), or a weak non-electrostatic attraction develops at high  $\phi$ .

Using the same values for  $Z_\infty$  we also predict the correct sedimentation–diffusion equilibrium density profiles (equation (6.1) and figure 5(a)). Finally, we note that we have used the same values for the charge at infinite dilution  $Z_\infty$  as in [63] and the same values for  $\kappa^{-1}$  and  $n_\infty$  as in [26, 66].

In conclusion, assuming regulation of the charge of silica colloids upon compression, we obtain a very accurate description of the osmotic pressure of colloidal silica in ethanol, much better than when a fixed charge is assumed. Up to a particle volume fraction of at least 1%, no further corrections are required to describe the data. On a double-logarithmic

scale the experimental  $\Pi_c(\phi)$  data follow a characteristic S-shaped curve, which is accurately reproduced only by the charge-regulation model. These findings suggest that silica particles indeed reduce their surface charge when they are being concentrated [63, 71], and that charge regulation should be included in an accurate model for the equation of state of silica in ethanol, and, most likely, in other suspensions of charged colloids as well.

## 7. Application to dumbbells, trimers and colloidal chains

In this final section we briefly address the particle shape as an important factor in the SDE profiles and their dynamic development. For multicomponent suspensions of rods or disks, we give the relevant expressions for the chemical potential, based on previous reports, in the supporting information.

For multicomponent systems containing one or more particle types that consist of hard spherical particles (beads) that are connected into dumbbells (dimers, consisting of two beads) [78, 79], trimers (three beads) [61] or short chains of  $N$  particles ( $N$  beads) [80], we propose a simple modification of the BMCSL theory and the power series as given in section 4, namely we correct the terms that account for the translational entropy of the connected particles in equations (4.1) and (4.3) with a  $1/N_i$  term, i.e. the ideal term  $\ln \phi_i$  and the term for these particles in  $\xi_0$ . This approach is common in Flory–Huggins polymer theory and has been suggested before in [81]. As a result, in the polydisperse mixture the parameter  $\xi_0$  (equations (4.4) and (4.5)) will change according to:

$$\xi_{0,N} = \sum_j \phi_j \sigma_j^{-3} N_j^{-1} \quad (7.1)$$

and the ideal entropy term  $(\phi_i/v_i) \ln(\phi_i/v_i)$  in equation (4.1) will change to  $(\phi_i/N_i v_i) \ln(\phi_i/v_i)$ . The other terms, which account for excluded volume interactions, will remain unchanged, assuming that the volume excluded by two connected hard spheres is equal to the volume excluded by two separate hard spheres of equal size. Thus, using the definition of the chemical potential:  $\mu_i = v_i(\partial f/\partial \phi_i)$  and  $(\partial \xi_{0,N}/\partial \phi_i) = (\xi_{0,N}/N_i \sigma_i^3)$ , we can derive the following expression for the excess chemical potential *per bead* of species  $i$  in a polydisperse mixture according to the BMCSL equation of state,

$$\begin{aligned} \frac{\mu_{i,N}^{\text{exc}}}{k_B T} = & - \left( \frac{1}{N_i} + \frac{2\xi_2^3 \sigma_i^3}{\phi^3} - \frac{3\xi_2^2 \sigma_i^2}{\phi^2} \right) \ln(1-\phi) \\ & + \frac{3\xi_2 \sigma_i + 3\xi_1 \sigma_i^2 + \xi_{0,N} \sigma_i^3}{1-\phi} + \frac{3\xi_2^2 \sigma_i^2}{\phi(1-\phi)^2} \\ & + \frac{3\xi_1 \xi_2 \sigma_i^3}{(1-\phi)^2} - \xi_2^3 \sigma_i^3 \frac{\phi^2 - 5\phi + 2}{\phi^2(1-\phi)^3}. \end{aligned} \quad (7.2)$$

Following the same strategy as in section 4 we can write equation (7.2) as a series of powers of  $\phi$ :

$$\begin{aligned} \frac{\mu_{i,N}^{\text{exc}}}{k_B T} = & \sum_{\lambda=1}^{\infty} \left[ \left( \lambda^2 - 2\lambda - 1 + \frac{2}{\lambda} \right) A^3 + 3 \left( \lambda - \frac{1}{\lambda} \right) A^2 \right. \\ & \left. + 3(\lambda-1)AB + 3A + 3B + C_N + \frac{1}{\lambda N_i} \right] \phi^\lambda \end{aligned} \quad (7.3)$$

where  $C_N = \sum_j \alpha_{ij}^3 \zeta_j / N_j$ . The derivation of this series is given in the supporting information. In the case that we have only two species (monomers and  $N$ -mers) and the fraction of  $N$ -mers is very small:  $\phi_N \ll \phi_1$ :

$$\begin{aligned} \frac{\mu_N^{\text{exc}}}{k_B T} = & \sum_{\lambda=1}^{\infty} \left[ (1+\lambda\alpha)^3 + 3(\lambda-1)\alpha^2 \right. \\ & \left. + (\lambda-1)(\lambda-2)\alpha^3 - 1 + \frac{1}{N} \right] \frac{\phi_1^\lambda}{\lambda}. \end{aligned} \quad (7.4)$$

In figure 6 we show the effect of the connectivity of particles on the SDE profiles. As expected, SDE profiles of dimers, trimers and, in general,  $N$ -mers extend less far than SDE profiles of monomeric particles. The translational entropy that opposes the effect of gravity is smaller for the clusters than for monomers. The effect is, however, small and the separation of the clusters will be even smaller in a strong centrifugal field (assuming all clusters have the same density  $\rho_c$ ). As a consequence, it is, in practice, very difficult to separate clusters of the same density but of different size, in a simple sedimentation experiment or by centrifugation (see section 5) [61]. Instead, separation of these clusters during dynamic centrifugation relies on differences in sedimentation velocity caused by differences in the effective cross-sectional area of the clusters.

## 8. Concluding remarks

Sedimentation of proteins, colloids, and larger particulate matter remains an intriguing and inspiring topic. We argue that the suspension density must be used to calculate the buoyancy force. As a result of canceling terms in the gravitational (centrifugal) force and the thermodynamic force or potential, the equilibrium sedimentation profiles can be calculated using the difference between the density of the sedimenting particles and the fluid. Nonetheless, many experimental phenomena in sedimenting systems require the consideration that the suspension density is the buoyant density. We have given a general theoretical framework that can be used to calculate both equilibrium sedimentation profiles and their dynamic development, under the assumption of local thermal equilibrium, for any kind of particles and mixtures of particles.

We have shown examples for mixtures of hard spheres, clusters of spheres and for suspensions of charged particles. For suspensions of hard spheres to which a trace amount of another type of particle is added, the theory can be simplified using an elegant power series of the BMCSL equation of state. We have shown that this expression yields predictions for the entire density profiles of the tracer particles that are in perfect agreement with experiments. In multicomponent mixtures outside the tracer limit, the full theory must be used and we have shown that it predicts interesting cases of sedimentation banding for hard spheres of different sizes and densities. We extended our theory to charged particles, and spheres that are connected into dimers, trimers and short chains. Our approach is not limited to particles in a certain size range. It can be applied to mixtures, to hard and charged

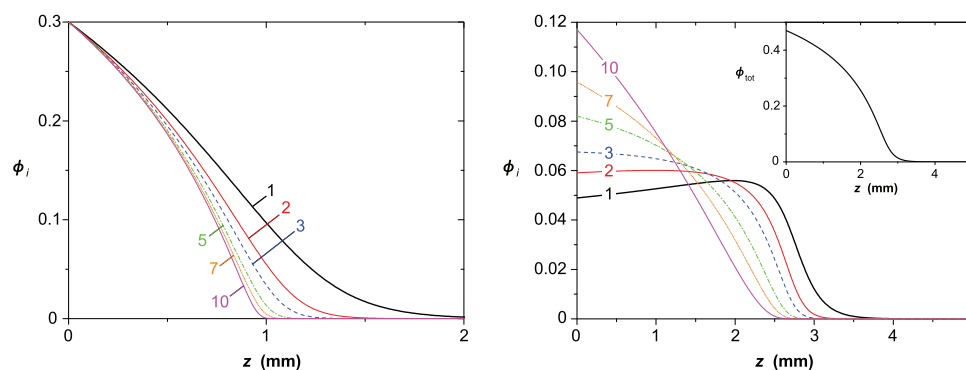


**Figure 6.** (a) Theoretical predictions (equations (4.1) and (7.2)) of the equilibrium sedimentation profiles of a suspension of hard spheres (beads) ( $\sigma = 300$  nm,  $\rho = 1.19$  g cm $^{-3}$ ) that are either unconnected (monomers, label 1) or connected together as dimers (2), trimers (3), pentamers (5), heptamers (7) or decamers (10), each in a solution with  $\rho_F = 1.04$  g cm $^{-3}$ . For each profile the equilibrium volume fraction at  $z = 0$  is fixed at  $\phi = 0.30$ . (b) As in (a), but for a mixture of monomers, dimers, trimers, pentamers, heptamers and decamers, with for each type the same amount. The inset shows the cumulative volume fraction profile of this multicomponent mixture.

particles, and it covers both equilibrium sedimentation profiles and their dynamic development.

For soft, compressible particles and strongly interacting particles, our general theoretical framework might serve as a basis for a further generalization of the concept of buoyancy. We believe that our formulation of the buoyancy force as a pressure gradient and the thermodynamic force as a gradient of the (total) potential and the gradient of the osmotic pressure (see section 3) opens the possibility to define buoyancy and describe sedimentation for particles without a well-defined volume, such as star-shaped polymers and compressible microgel beads, and for particles that are strongly interacting.

## Acknowledgments

ES and PMB gratefully acknowledge R Piazza (Politecnico di Milano, Italy) for providing experimental data and inspiring discussions and F A M Leermakers (Wageningen University, The Netherlands) and J W Zwanikken (Northwestern University, USA) for inspiring discussions as well.

## References

- [1] Piazza R, Buzzaccaro S and Parola A 2012 *Soft Matter* **8** 7112–5
- [2] Piazza R, Buzzaccaro S and Secchi E 2012 *J. Phys.: Condens. Matter* **24** 284109
- [3] Ball P 2012 *Nature Mater.* **11** 488
- [4] Dijkstra J A, Wandersman E, Slotterback S, Berardi C R, Updegraff W D, Van Hecke M and Losert W 2010 *Phys. Rev. E* **82** 060301
- [5] Jamie E A G, Wensink H H and Aarts D G A L 2010 *Soft Matter* **6** 250–5
- [6] Beveridge T 2002 *Crit. Rev. Food Sci. Nutr.* **42** 317–37
- [7] Kästner U 2001 *Colloids Surf. A* **183–185** 805–21
- [8] Frey P and Church M 2009 *Science* **325** 1509–10
- [9] Bai L, Ma X, Liu J, Sun X, Zhao D and Evans D G 2010 *J. Am. Chem. Soc.* **132** 2333–7
- [10] Richardson J and Meikle R 1961 *Trans. Inst. Chem. Eng.* **39** 348–56
- [11] Masliyah J H 1979 *Chem. Eng. Sci.* **34** 1166–8
- [12] Foscolo P U, Gibilaro L G and Waldrum S P 1983 *Chem. Eng. Sci.* **38** 1251–60
- [13] Patwardhan V S and Tien C 1985 *Chem. Eng. Sci.* **40** 1051–60
- [14] Poletto M and Joseph D D 1995 *J. Rheol.* **39** 323–43
- [15] van der Wielen L A M, van Dam H M and Luyben K C A M 1996 *Chem. Eng. Sci.* **51** 995–1008
- [16] Biesheuvel P M, Verweij H and Breedveld V 2001 *Am. Inst. Chem. Eng. J.* **47** 45–52
- [17] Biesheuvel P M, Verweij H and Breedveld V 2001 *Am. Inst. Chem. Eng. J.* **47** 1969–77
- [18] Gibilaro L G, Waldrum S P and Foscolo P U 1984 *Chem. Eng. Sci.* **39** 1819–20
- [19] Gibilaro L G, Di Felice R and Waldrum S P 1987 *Chem. Eng. Sci.* **42** 194–6
- [20] Gibilaro L G, Foscolo P U, Di Felice R and Waldrum S P 1987 *Chem. Eng. Sci.* **42** 1272
- [21] Piazza R, Buzzaccaro S, Secchi E and Parola A 2013 *Phys. Biol.* **10** 045005
- [22] Jackson G, Rowlinson J S and van Swol F 1987 *J. Phys. Chem.* **91** 4907–12
- [23] Martin M, Hoyos M and Lhuillier D 1994 *Colloid Polym. Sci.* **272** 1582–9
- [24] Batchelor G 1976 *J. Fluid Mech.* **74** 1–29
- [25] Belloni L 2005 *J. Chem. Phys.* **123** 204705
- [26] Raşa M and Philipse A P 2004 *Nature* **429** 857–60
- [27] Biesheuvel P M and Lyklema J 2005 *J. Phys.: Condens. Matter* **17** 6337–52
- [28] Kops-Werkhoven M, Vrij A and Lekkerkerker H 1983 *J. Chem. Phys.* **78** 2760–3
- [29] Vrij A 1980 *J. Chem. Phys.* **72** 3735–9
- [30] Biben T, Hansen J P and Barrat J L 1993 *J. Chem. Phys.* **98** 7330–44
- [31] Wills P R, Jacobsen M P and Winzor D J 1996 *Biopolymers* **38** 119–30
- [32] Wensink H H and Lekkerkerker H N W 2004 *Europhys. Lett.* **66** 125–31
- [33] Parola A, Buzzaccaro S, Secchi E and Piazza R 2013 *J. Chem. Phys.* **138** 114907
- [34] Astarita G 1993 *Chem. Eng. Sci.* **48** 3438–40
- [35] Earl of Berkeley and Hartley E G J 1909 *Proc. R. Soc. Lond. A* **82** 271–5
- [36] Mauro A 1957 *Science* **126** 252–3
- [37] Ray P M 1960 *Plant Physiol.* **35** 783–95
- [38] Fair J C and Osterle J F 1971 *J. Chem. Phys.* **54** 3307–16

- [39] Osterle J F and Pechersky M J 1971 *J. Phys. Chem.* **75** 3015–20
- [40] Peppin S, Elliot J and Worster M 2005 *Phys. Fluids* **17** 053301
- [41] Biesheuvel P M 2011 *J. Colloid Interface Sci.* **355** 389–95
- [42] Cartwright J H E, Escibano B, González D L, Sainz-Díaz C I and Tuval I 2013 *Langmuir* **29** 7655–60
- [43] Dhont J 2004 *J. Chem. Phys.* **120** 1632–41
- [44] Biesheuvel P M 2000 *Chem. Eng. Sci.* **55** 2595–606
- [45] Biesheuvel P M 2000 *Chem. Eng. Sci.* **55** 1945–7
- [46] Morganthaler J J and Price C A 1976 *Biochem. J.* **153** 487–90
- [47] Boublik T 1970 *J. Chem. Phys.* **53** 471–2
- [48] Mansoori G A, Carnahan N F, Starling K E and Leland T W 1971 *J. Chem. Phys.* **54** 1523–5
- [49] Biesheuvel P and van Soestbergen M 2007 *J. Colloid Interface Sci.* **316** 490–9
- [50] Hill T L 1962 *Statistical Thermodynamics* (Reading, MA: Addison-Wesley)
- [51] Bikerman J J 1942 *Phil. Mag.* **33** 384–97
- [52] Biben T and Hansen J P 1993 *Mol. Phys.* **80** 853–9
- [53] Schmidt M, Dijkstra M and Hansen J P 2004 *J. Phys.: Condens. Matter* **16** S4185–94
- [54] Cuny G, Soriano P, Macaya G and Bernardi G 1981 *Eur. J. Biochem.* **115** 227–33
- [55] Modak S P, Imaizumi M T, Chappuis M and Scherrer K 1978 *Mol. Biol. Rep.* **4** 55–60
- [56] Price C W, Leslie D C and Landers J P 2009 *Lab Chip* **9** 2484–94
- [57] Lebowitz J, Lewis M S and Schuck P 2002 *Protein Sci.* **11** 2067–79
- [58] Balbo A, Minor K H, Velikovskiy C A, Mariuzza R A, Peterson C B and Schuck P 2005 *Proc. Natl Acad. Sci. USA* **102** 81–6
- [59] Xiong B, Cheng J, Qiao Y, Zhou R, He Y and Yeung E S 2011 *J. Chromatogr. A* **1218** 3823–9
- [60] Svedberg T and Pedersen K O 1940 *The Ultracentrifuge* (Oxford: Clarendon)
- [61] Manoharan V N, Elsesser M T and Pine D J 2003 *Science* **301** 483–7
- [62] Sharma V, Park K and Srinivasarao M 2009 *Proc. Natl Acad. Sci. USA* **106** 4981–5
- [63] Biesheuvel P M 2004 *J. Phys.: Condens. Matter* **16** L499–504
- [64] Dijkstra M, Zwanikken J and van Roij R 2006 *J. Phys.: Condens. Matter* **18** 825
- [65] Cuetos A, Hynninen A P, Zwanikken J, Dijkstra M and van Roij R 2006 *Phys. Rev. E* **73** 061402
- [66] Raša M, Erné B H, Zoetekauw B, van Roij R and Philipse A P 2005 *J. Phys.: Condens. Matter* **17** 2293–314
- [67] Hachisu S and Takano K 1982 *Adv. Colloid Interface Sci.* **16** 233–52
- [68] Russel W B, Saville D A and Schowalter W R 1989 *Colloidal Dispersions* (Cambridge: Cambridge University Press)
- [69] Barrat J L, Biben T and Hansen J P 1992 *J. Phys.: Condens. Matter* **4** L11–4
- [70] Piazza R, Bellini T and Degiorgio V 1993 *Phys. Rev. Lett.* **71** 4267–70
- [71] Simonin J P 1995 *J. Phys. Chem.* **99** 1577–81
- [72] Rutgers M A, Dunsmuir J H, Xue J Z, Russel W B and Chaikin P M 1996 *Phys. Rev. B* **53** 5043–6
- [73] Zwanikken J and van Roij R 2005 *Europhys. Lett.* **71** 480–6
- [74] Philipse A P and Koenderink G H 2003 *Adv. Colloid Interface Sci.* **100–102** 613–39
- [75] van Roij R 2003 *J. Phys.: Condens. Matter* **15** S3569–80
- [76] Philipse A P 2004 *J. Phys.: Condens. Matter* **16** S4051–62
- [77] Trizac E and Levin Y 2004 *Phys. Rev. E* **69** 031403
- [78] Peng B, Vutukuri H R, van Blaaderen A and Imhof A 2012 *J. Mater. Chem.* **22** 21893–900
- [79] Peng B, Smalenburg F, Imhof A, Dijkstra M and van Blaaderen A 2013 *Angew. Chem. Int. Edn* **52** 6709–12
- [80] Vutukuri H R, Demirörs A F, Peng B, van Oostrum P D J, Imhof A and van Blaaderen A 2012 *Angew. Chem. Int. Edn* **51** 11249–53
- [81] de Vos W M, Biesheuvel P M, de Keizer A, Kleijn J M and Cohen Stuart M A 2009 *Langmuir* **25** 9252–61
- [82] Taylor R and Krishna R 1993 *Multicomponent Mass Transfer* (New York: Wiley)
- [83] Lightfoot E N 1974 *Transport Phenomena and Living Systems: Biomedical Applications of Momentum and Mass Transfer* (New York: Wiley)